Theory of Noise and Transfer Properties of IMPATT Diode Amplifiers

JASPER J. GOEDBLOED AND MARINUS T. VLAARDINGERBROEK, SENIOR MEMBER, IEEE

Abstract—**A theory is formulated which describes quantitatively the noise and transfer properties of IMPATT diode reflection-type negative resistance amplifiers. This theory is based on the method used in the large-signal theory of noise in IMPATT diode oscillators by the present authors. The theory takes into account the signal dependence of the noise generation in the diode, the noise and/or modulation present in the input signal, and also the intermodulation effects occurring between the various frequency bands. The equations are conveniently arranged in matrix form; such a formulation makes it easier to obtain quantitative results in terms of measurable noise and modulation parameters. Agreement between measured and theoretically predicted AM and FM noise of injection-locked oscillators is good. The usefulness of the theory is illustrated by results of calculations on minimum attainable noise of a given amplifier, maximum noise allowable on the input signal, AM–FM conversion, phase distortion, bias modulation, and the correlation between various types of noise.**

I. Introduction

REFLECTION-TYPE negative resistance amplifiers, used for the amplification of frequency-modulated or phase-modulated signals, have recently found application in microwave FM and PCM radio relay links. The active devices in such amplifiers are Gunn or IMPATT diodes. If low noise plus low output power requirements have to be fulfilled, a Gunn diode can be chosen. However, when high power levels are required the IMPATT diode is used. Since an IMPATT diode is inherently noisy, such an amplifier has to be carefully designed and, consequently, a way of describing the noise properties of the amplifier is needed. This description should be based on a detailed understanding of the large-signal noise generation mechanism in the diode [1]–[7]. It is the aim of the present paper to use results of these studies in a quantitative description of the noise and transfer properties of negative resistance amplifiers, including the practical circuitry of the amplifier.

There are two types of negative resistance amplifiers, namely, the stable amplifier and the injection-locked oscillator. Although both types of amplifiers have practical differences, the theoretical description is analytically identical. Following the pioneering work of Adler [8],much work has been done to clarify the behavior of both types of amplifiers. A comprehensive survey has been published by Kurokawa [9]. In these analyses the current through the device is assumed to be AM and FM modulated, due to the noise perturbations generated in the device and possibly in the input source, as seen from $I(t) = \{A_0 + a(t)\} \times \sin\{\omega_0 t + \phi(t)\}$. This current is introduced in the appropriate loop equation, which is subsequently developed in a Taylor series around the unperturbed situation, as characterized by $I_0(t) = A_0 \sin(\omega_0 t + \phi_0)$. Although this method gives a wealth of physical understanding, it becomes very difficult to obtain quantitative results if 1) the active device in the amplifier has an impedance with both the real and imaginary part depending on the signal amplitude and frequency, if 2) the noise far away from the carrier has to be described, and if 3) the noise (or modulation) of the input signal has to be included. We have therefore based our quantitative description of the noise and transfer properties of the amplifiers on the same mathematical approach successfully used earlier in our study of IMPATT diode oscillator noise [3] and the generation of parametric instabilities in these oscillators [10]–[12]. Basically, the approach starts with a noise-free amplifier, operating at the frequency ω_L, which is subsequently modulated by small perturbation signals at frequencies $\omega_L \pm \Omega$ and Ω, where in terms of AM and FM noise the low-frequency component $\Omega(= 2\pi f_m)$ is called the "distance from carrier." The perturbation signals are assumed to be due to 1) the noise generated in the IMPATT diode, 2) the noise or modulation of the input signal, and 3) the noise or modulation of the diode bias current.

The paper will be organized in the following way. In Section II the most elementary equivalent circuit of a negative resistance amplifier is considered with respect to the stable noise-free solution and the perturbations in the sidebands. In Section III this elementary theory is applied to a practical circulator-coupled amplifier, taking the practical circuitry into account. Use is made of the Read diode model to describe the nonlinearity of the diode. The method used allows for application of more extended [13], [22] or other [14] descriptions of the nonlinearity. However, as will be shown in Section IV, measured results are quantitatively described by the present theory. Finally, in Section V some transfer properties of the amplifier will be discussed.

II. Theory

Fig. 1 gives an equivalent circuit of the simplest negative resistance amplifier. The active device is characterized by its impedance Z_d, which, in the case of an IMPATT diode, is a known nonlinear function of the bias current, the angular frequency ω, and the ac signal present. The load is characterized by the frequency-dependent impedance $Z_e(\omega)$,

Manuscript received June 1, 1976; revised September 15, 1976.

J. J. Goedbloed is with Philips Research Laboratories, Eindhoven, The Netherlands.

M. T. Vlaardingerbroek is with the Development Laboratories for Transmitting Tubes and Microwave Components, N. V. Philips' Gloeilampenfabrieken, Product Division Elcoma, Eindhoven, The Netherlands.

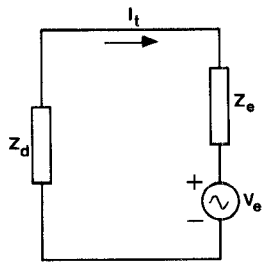

Fig. 1. Equivalent circuit of a simple negative resistance amplifier.

and the input signal by a series ac voltage source of frequency ω and amplitude V_e.

To describe the noise and transfer properties of the amplifier, a noise-free amplifier with input signal of frequency $\omega_L = 2\pi f_L$ is considered first, which is subsequently perturbed by signals at the frequencies ω_k, where $\omega_k = \omega_L + k\Omega$ for $k = \pm 1$, and $\omega_k = \Omega = 2\pi f_m$ for $k = 0$. In Section II-A we give a summary of the nonlinearity and noise generation in the avalanche region, described in detail in [3]. In Section II-B the loop as given in Fig. 1 will be discussed.

A. Nonlinearity and Noise of the Avalanche Region

The diode model used is the Read diode model, i.e., the only nonlinearity considered is that due to the nonlinear response of the avalanche process as described by Read's equation

$$\frac{d}{dt} I_{ca}(t) = I_{ca}(t) \frac{d}{dt} U(t) + \frac{1}{\tau_i} g'(t) \tag{1}$$

where

$$U(t) = \frac{\bar{\alpha}'}{\tau_i} \int_{t_0}^{t} V_a(\tau)\, d\tau$$

and where $I_{ca}(t)$ is the conduction current in the avalanche region caused by the voltage $V_a(t)$ across that region, and $g'(t)$ the Langevin term describing the noise generation. The field derivative of the average ionization coefficient is denoted by $\bar{\alpha}'$, and τ_i is the intrinsic response time of the avalanche process [15]. For the unperturbed stationary situation, indicated by capitals with index 0, the solution of (1) is

$$I_{ca0}(t) = I_B \sum_{n=-\infty}^{\infty} M_n(U_0) \exp(jn\omega_L t) \tag{2}$$

where $V_{a0}(t)$ is assumed to be sinusoidal. In (2), I_B is the bias current supplied from a constant current source, and

$$M_n(U_0) = M_n = I_n(U_0)/I_0(U_0) \tag{3}$$

where $I_n(U_0)$ is the nth order modified Bessel function with argument $U_0 = (\bar{\alpha}' V_{a0})/(\omega_L \tau_i)$.

Proceeding as in [3], in the presence of perturbations the solution of (1) yields for the lowest order mixing terms with positive Ω at the spectral components ω_k mentioned previously, the vector equation

$$\begin{bmatrix} i^*_{ca-1} \\ i_{ca0} \\ i_{ca1} \end{bmatrix} = \begin{bmatrix} 1 & M_1 & M_2 \\ M_1 & 1 & M_1 \\ M_2 & M_1 & 1 \end{bmatrix} \begin{bmatrix} I_B u^*_{-1} + g^*_{-1} \\ I_B u_0 + g_0 \\ I_B u_1 + g_1 \end{bmatrix} \tag{4}$$

where the perturbing quantities are indicated by a lower case letter, and the asterisk means complex conjugate. Equation (4) can be abbreviated to

$$\boldsymbol{i}_{ca} = \boldsymbol{M}(I_B \boldsymbol{u} + \boldsymbol{g}). \tag{4a}$$

The element g_k of the column vector $\boldsymbol{g}$ is given by

$$g_k = \left\{ \frac{qI_B B I_0^2(U_0)}{\omega_k^2 \tau_i^2} \right\}^{1/2} \tag{5}$$

where q is the electronic charge and B the bandwidth considered. In practical situations the noise generation may depart from the $I_0^2(U_0)$ dependence due to the generation of an extra saturation current in the diode, as discussed in [5]–[7].

Equation (4) gives the relation between the perturbing conduction current in the avalanche region ($\boldsymbol{i}_{ca}$), the noise generated in that region ($\boldsymbol{g}$), and the perturbing voltage across that region ($\boldsymbol{u}$). In contrast to the case of the free-running oscillator [3], $\boldsymbol{u}$ may now consist of two parts: a part caused by $\boldsymbol{g}$ and a part caused by the perturbing signals present in the input signal.

B. Total Current in the Amplifier Loop

The equation for the total current I_t in the amplifier loop is obtained by adding to the equation for the conduction current, derived in Section II-A, equations for the capacitive current, the drift region, and the total voltage drop in the loop. For the unperturbed signal this is a well-known procedure, so that the unperturbed stationary condition is defined by

$$I_{t0}(\omega_L)\{Z_d(\omega_L, I_B, U_0) + Z_e(\omega_L)\} + V_{e0} \exp(j\phi_e) = 0 \tag{6}$$

where, on account of the assumptions made,

$$I_{t0}(\omega_L) = I_{ca0}(\omega_L)\{1 - \omega_L^2/\omega_a^2\} \tag{7}$$

$$Z_d(\omega_L) = \frac{1}{j\omega_L C_0} - \frac{\Phi(\omega_L)}{j\omega_L C_d} \cdot \frac{1}{1 - \omega_L^2/\omega_a^2} \tag{8}$$

$$\omega_a^2/\omega_{a0}^2 = 2M_1(U_0)/U_0 \tag{9}$$

and ϕ_e is the phase difference between I_{t0} and the input signal V_{e0}. In (8), C_0 and C_d are the "cold" capacitance of the depletion layer and the drift region, respectively. $\Phi(\omega_L)$ is the transit time function defined by

$$\Phi(\omega_L) = l_a/l_d + \{1 - \exp(-j\theta)\}/j\theta$$

where l_a and l_d are the lengths of the avalanche region and of the drift region, respectively, and $\theta = \omega_L \tau_d$, where τ_d is the transit time of the carriers in the drift region. In (9), ω_{a0} is the small-signal avalanche frequency defined by $\omega_{a0}^2 = (\bar{\alpha}' I_B)/(\tau_i C_a)$, where C_a is the cold capacitance of the avalanche region.

For given values of I_B, ω_L, and V_{e0} the nonlinear equation (6) can be solved numerically [16] so as to yield I_{t0} and ϕ_e. In the case of a locked oscillator with ω_L equal to the free-running oscillation frequency ω_f, it is easily shown that

$$\tan(\phi_e) = \text{Re}\{\Phi(\omega_L)\}/\text{Im}\{\Phi(\omega_L)\}$$

which condition can be used to verify the calculations.

Again proceeding as in [3], the total perturbing loop currents i_{tk} on I_t follow after straightforward calculation to be given by the vector equation

$$\begin{bmatrix} 1+(1-\beta_{-1}^2)S_{-1}^* & -\beta_0^2 M_1 S_0 & -\beta_1^2 M_2 S_1 \\ -\beta_{-1}^2 M_1 S_{-1}^* & 1+(1-\beta_0^2)S_0 & -\beta_1^2 M_1 S_1 \\ -\beta_{-1}^2 M_2 S_{-1}^* & -\beta_0^2 M_1 S_0 & 1+(1-\beta_1^2)S_1 \end{bmatrix} \begin{bmatrix} i_{t-1}^* \\ i_{t0} \\ i_{t1} \end{bmatrix} = \begin{bmatrix} 1 & M_1 & M_2 \\ M_1 & 1 & M_1 \\ M_2 & M_1 & 1 \end{bmatrix} \begin{bmatrix} g_{-1}^* \\ g_0 \\ g_{-1} \end{bmatrix} + \begin{bmatrix} -(1-\beta_{-1}^2)F_{-1}^* & \beta_0^2 M_1 F_0 & \beta_1^2 M_2 F_1 \\ \beta_{-1}^2 M_1 F_{-1}^* & -(1-\beta_0^2)F_0 & \beta_1^2 M_1 F_1 \\ \beta_{-1}^2 M_2 F_{-1}^* & \beta_0^2 M_1 F_0 & -(1-\beta_1^2)F_1 \end{bmatrix} \begin{bmatrix} v_{e-1}^* \\ v_{e0} \\ v_{e1} \end{bmatrix} \quad (10)$$

where

$$\beta_k^2 = \omega_{a0}^2/\omega_k^2$$

$$S_k = \frac{j\omega_k C_d Z_e(\omega_k) + (l_a + l_d)/l_d}{\Phi(\omega_k)} - 1 \quad (11)$$

and

$$F_k = j\omega_k C_d/\Phi(\omega_k). \quad (12)$$

Equation (10) can be abbreviated by using vector notation

$$\boldsymbol{S}\boldsymbol{i}_t = \boldsymbol{M}\boldsymbol{g} + \boldsymbol{F}\boldsymbol{v}_e \quad \text{or} \quad \boldsymbol{i}_t = \boldsymbol{S}^{-1}\boldsymbol{M}\boldsymbol{g} + \boldsymbol{S}^{-1}\boldsymbol{F}\boldsymbol{v}_e. \quad (12a)$$

Equations (10) and (12a) relate the perturbation currents i_{tk} imposed on the total unperturbed loop current $I_{t0}(\omega_L)$ to the noise generated by the avalanche process, described by $\boldsymbol{g}$, *and* to the noise or modulation present in the input signal, described by $\boldsymbol{v}_e$. When $\boldsymbol{v}_e \equiv 0$, (12a) is identical to the equation for $\boldsymbol{i}_t$ in the case of a free-running oscillator [3, eq. (20a)]. However, in general, the noise current of a free-running oscillator will be much larger than that of an amplifier. In the present description this difference is found again when considering det $\{\boldsymbol{S}\}$, which is used in the inversion of $\boldsymbol{S}$. In case of a free-running oscillator det $\{\boldsymbol{S}\}$ is nearly zero, when considering perturbations not too far away from the carrier, since $Z_d(\omega_f) = Z_e(\omega_f)$. This causes high values of i_{tk}. In the case of the amplifier $Z_d(\omega_L) \neq Z_e(\omega_L)$ because of the input signal present, resulting in det $\{\boldsymbol{S}\} \neq 0$, and hence in lower values of i_{tk}.

Since knowledge is only available of the main square value of the noise quantities involved, $\boldsymbol{i}_t$ in (12a) must be multiplied by its Hermitian conjugate, to be indicated by the dagger†. Subsequently, the elements of the matrix $\boldsymbol{i}_t\boldsymbol{i}_t^\dagger$ must be averaged over a time interval which is long compared with the period of the frequency Ω. We thus find the formal solution of our problem

$$\langle \boldsymbol{i}_t\boldsymbol{i}_t^\dagger \rangle = \boldsymbol{S}^{-1}\boldsymbol{M}\langle \boldsymbol{g}\boldsymbol{g}^\dagger \rangle \boldsymbol{M}^\dagger (\boldsymbol{S}^{-1})^\dagger + \boldsymbol{S}^{-1}\boldsymbol{F}\langle \boldsymbol{v}_e\boldsymbol{v}_e^\dagger \rangle \boldsymbol{F}^\dagger (\boldsymbol{S}^{-1})^\dagger \quad (13)$$

where the brackets denote the averaging, and where it has been assumed that there is no correlation between $\boldsymbol{g}$ and $\boldsymbol{v}_e$. It will be assumed that all off-diagonal elements of the matrix $\langle \boldsymbol{g}\boldsymbol{g}^\dagger \rangle$ are zero, indicating that complete randomness of the occurrence of the generation of electron-hole pairs is assumed (white noise).

The theory is easily extended to include many more perturbing signal frequencies than the three frequencies ω_k considered here. However, since even the exact waveform on the avalanche region is unknown, it is thought to be useless to go into more detail. The general trend will be well described by the present theory, except at the highest power levels, where the large-signal model used needs extension [13], [14]. When spurious parametric signals are to be considered it is sufficient to consider perturbations at the frequencies Ω and $\omega_L - \Omega$ only [11], [12]. As will be clear from inspection of (12a), the onset of spurious signals is determined by det $\{\boldsymbol{S}\} = 0$, as in the case of a free-running oscillator [10]. This is in agreement with experimental observations [10], [11].

III. Application to a Practical Circulator-Coupled Amplifier

In practice, the amplifier is much more complicated than suggested in Fig. 1, due to the necessity of separating the input and output circuits with a circulator. A practical amplifier circuit is shown in Fig. 2, where it is assumed that the input branch I and the output branch III are matched to the circulator having an input impedance Z_0. For convenience of argument, the circulator is assumed to be lossless. The IMPATT diode as active element, and represented in branch II by Z_d, is coupled to the circulator by the transformation network T. This network contains the diode series resistance, the mounting parasitics, the circuit losses and the transformer. In order to obtain a relation between the measurable perturbing (noise and/or modulation) quantities in the input circuit and those in the output circuit, taking the noise generation in the diode into account, the unperturbed currents and voltages are considered first.

The amplitude of the series input voltage source V_{i0} of frequency ω_L is related to the input power $P_i(\omega_L)$ according to $V_{i0} = (8P_iZ_0)^{1/2}$. The current in the output circuit $I_{00}(\omega_L)$ is related to the input signal via the relation [cf. Fig. 2(a)]

$$I_{00}(\omega_L) = I_{L0}(\omega_L) - V_{i0}(\omega_L)/2Z_0 \quad (14)$$

which is suggested by a consideration of the total current flowing into the circulator and follows from application of the power wave concept [17]. Next $I_{L0}(\omega_L)$ in (14) has to be eliminated, and the connection with the theory of Section II has to be made. For this purpose two equivalent circuits of branch II are considered: one at the reference plane *aa'* as shown in Fig. 2(b), and one at the reference plane *bb'* [Fig. 2(c)]. The circuit of Fig. 2(b) is identical to that in Fig. 1; V_{e0} represents the input signal and Z_e the load impedance. In the circuit of Fig. 2(c) the input signal coming from branch I is represented by the series voltage

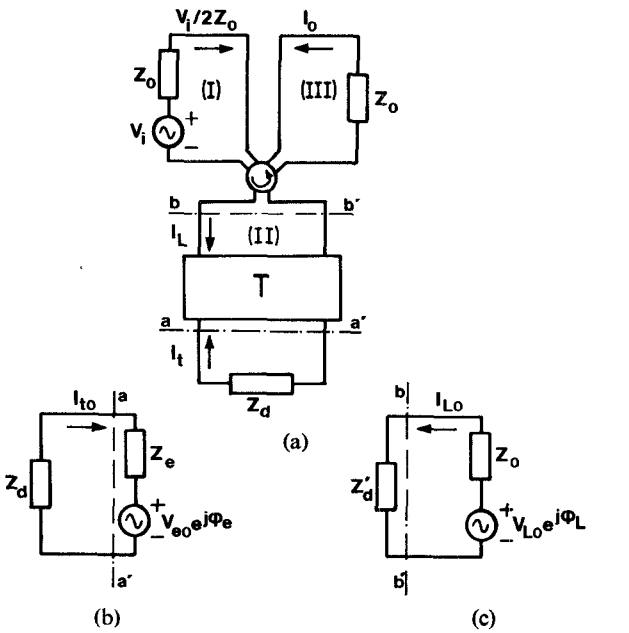

Fig. 2. (a) Circulator-coupled negative resistance amplifier. (b) Equivalent circuit of branch II at the reference plane aa' (capitals and index 0 indicate $\omega = \omega_L$ is considered). (c) Equivalent circuit of branch II at the reference plane bb' (capitals and index 0 indicates $\omega = \omega_L$ is considered).

source $V_{L0} \exp(j\phi_L)$, where according to the power wave concept [17] $V_{L0} = V_{i0}$, and ϕ_L accounts for the phase difference between V_{L0} and I_{L0}. The transformed diode impedance as seen from bb' is indicated by Z_d'. Using fourpole relations, it follows that the circuits of Fig. 2(b) and (c) are interconnected by the equations

$$I_{L0}(\omega_L) = T_A(\omega_L)V_{L0}(\omega_L) + T_B(\omega_L)I_{t0}(\omega_L) \quad (15)$$

$$V_{e0}(\omega_L) = -T_B(\omega_L)V_{L0}(\omega_L) \quad (16)$$

where, in the case the transformation network T is described by a simple 2 × 2 impedance matrix Z, it follows that [cf. Fig. 2(a)]

$$T_A(\omega) = \{Z_0 + Z_{bb}(\omega)\}^{-1}$$

$$T_B(\omega) = Z_{ba}(\omega)T_A(\omega).$$

Equations (6) and (14)–(16) fully describe the unperturbed stationary condition. Since the circuit of Fig. 2(c) is formally the same as that of Fig. 1, the stationary condition in this circuit can be calculated as described in Section II-B, yielding $I_{L0}(\omega_L)$ and ϕ_L. Substitution of $I_{L0}(\omega_L)$ in (14) yields $I_{00}(\omega_L)$. When (15) and (16) are used, the stationary condition in the diode loop [Fig. 2(b)] can now be calculated. An example of the interconnection between the currents and voltages discussed is given in the vector diagram of Fig. 3. As in the derivation of the basic equations in Section II-B, I_{t0} is positioned along the real axis. V_{e0} is shifted over an angle ϕ_e with respect to I_{t0} according to (6); V_{L0} is shifted over an angle β with respect to V_{e0} as a result of the transformation factor T_B in (16), etc.

Next we discuss the perturbation currents and voltages. Equations (14)–(16) are linear, and can be applied to any

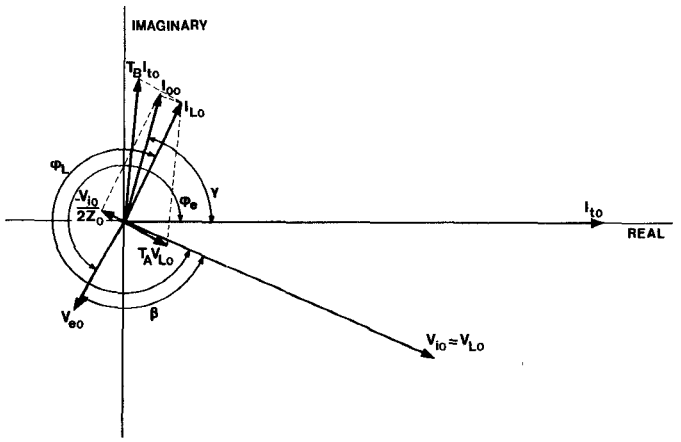

Fig. 3. Vector diagram in which the amplitudes and the phases of the various voltages and currents are represented in connection.

frequency and therefore to the defined frequencies ω_k as well. Then, again using the vector notation, for example, the corresponding equation of (15) becomes

$$\begin{bmatrix} i_{L-1}^* \\ i_{L0} \\ i_{L1} \end{bmatrix} = \begin{bmatrix} T_{A-1}^* & 0 & 0 \\ 0 & T_{A0} & 0 \\ 0 & 0 & T_{A1} \end{bmatrix} \begin{bmatrix} v_{L-1}^* \\ v_{L0} \\ v_{L1} \end{bmatrix} + \begin{bmatrix} T_{B-1}^* & 0 & 0 \\ 0 & T_{B0} & 0 \\ 0 & 0 & T_{B1} \end{bmatrix} \begin{bmatrix} i_{t-1}^* \\ i_{t0} \\ i_{t1} \end{bmatrix} \quad (17)$$

or

$$\boldsymbol{i}_L = \boldsymbol{T}_A\boldsymbol{v}_L + \boldsymbol{T}_B\boldsymbol{i}_t. \quad (17a)$$

Similarly,

$$\boldsymbol{i}_0 = \boldsymbol{i}_L - \boldsymbol{T}_c\boldsymbol{v}_i \quad (17b)$$

$$\boldsymbol{v}_L = \boldsymbol{v}_i \quad (17c)$$

$$\boldsymbol{v}_e = -\boldsymbol{T}_B\boldsymbol{v}_L \quad (17d)$$

where, due to the linearity of the equations, only diagonal terms occur, and where $T_{Ck} = 1/2Z_0$, $k = 0, \pm 1$. Substitution of (17a)–(17d) into (12a) yields, after elimination of $\boldsymbol{i}_t$, $\boldsymbol{i}_L$, $\boldsymbol{v}_e$, and $\boldsymbol{v}_L$,

$$\boldsymbol{i}_0 = \boldsymbol{T}_B\boldsymbol{S}^{-1}\boldsymbol{M}\boldsymbol{g} - (\boldsymbol{T}_B\boldsymbol{S}^{-1}\boldsymbol{F}\boldsymbol{T}_B - \boldsymbol{T}_A + \boldsymbol{T}_C)\boldsymbol{v}_i. \quad (18)$$

Equation (18) relates the output perturbing currents in the sidebands and at the low frequency, expressed by $\boldsymbol{i}_0$, with the input perturbing voltages $\boldsymbol{v}_i$, and the internally generated noise $\boldsymbol{g}$. A remark should be made on the low-frequency component. Often the low-frequency component of the input signal of a circulator-coupled amplifier will not enter branch II, nor therefore the diode loop [Fig. 2(b)]. This suggests that it is sufficient to consider the components at the frequencies $\omega_{\pm 1}$ only, thus reducing the vector dimensions from 3 to 2. However, the noise generation in the diode at the low frequency is still present, and this can influence, via upconversion, the noise in the sidebands at $\omega_{\pm 1}$. Hence no reduction of the equations is allowed. On the other hand, a perturbing voltage $v_B(\Omega)$ may be present in the bias current loop of the diode, which may cause upconverted perturbations. Therefore, the component v_{i0} of

v_i can successfully be replaced by $v_B(\Omega)$, when at the same time the transformation factors T_{A0}, T_{B0}, and T_{C0} are properly adjusted to represent the bias circuit. In this way, the effect of bias current modulation can be studied, while the component i_{00} of i_0 gives the total perturbing bias current. It should be noted that the problem discussed does not play a role in the theory of Section II, as $v_{e0}(\Omega)$ in that theory represents the bias modulation as well as the low-frequency component of the input signal.

In practice, the noise (and modulation) is expressed in terms of root-mean-square values of the amplitude and frequency fluctuations of the carrier signal and bias current fluctuations. The relation between the measurable noise quantities and, say, the perturbation currents i_0 of I_{00} can formally be written as

$$q_0 = T_0 i_0 \tag{19}$$

where q_0 is a column vector containing the measurable noise quantities. For example, when $i_c(\Omega)$ is the AM modulation current, and $\delta\omega(\Omega)$, the angular frequency deviation of I_{00} and $i_B(\Omega)$, is the bias noise current, then

$$q_0 = \begin{bmatrix} i_C(\Omega) \\ \delta\omega(\Omega) \\ i_B(\Omega) \end{bmatrix} = \begin{bmatrix} e^{+j\gamma} & 0 & e^{-j\gamma} \\ -j\Omega e^{+j\gamma}/I_{00} & 0 & j\Omega e^{-j\gamma}/I_{00} \\ 0 & \sqrt{2} & 0 \end{bmatrix} \begin{bmatrix} i_{0-1}^* \\ i_{00} \\ i_{01} \end{bmatrix} \tag{19a}$$

as can be derived in the same way as described in [3], [18]. In (19a) $\exp(-j\gamma)$ accounts for the phase angle between I_{t0} and I_{00} (see Fig. 3), since it has been assumed in the derivation of (18) that I_{t0} is along the real axis. Similarly, we define

$$q_i = T_i v_i \tag{20}$$

where the phase angle $(\phi_e + \beta)$ has to be taken into account (see Fig. 3). Substitution of (19) and (20) in (18) yields, after multiplying q_0 by its transpose conjugate and after averaging over a time interval which is long compared to the period of Ω,

$$\langle q_0 q_0^\dagger \rangle = G\langle g g^\dagger \rangle G^\dagger + Q\langle q_i q_i^\dagger \rangle Q^\dagger \tag{21}$$

where

$$G = T_0 T_B S^{-1} M$$

$$Q = T_0(T_B S^{-1} F T_B - T_A + T_C) T_i^{-1}.$$

In the next section this relation will be used to describe the noise of a practical locked oscillator.

We close this section with the following remarks.

1) Although the circulator was assumed to be lossless, the description can be extended to include the nonideal behavior of the circulator.

2) Equation (21) can be applied generally to locked oscillators, reflection-type amplifiers, and mutually coupled oscillators.

3) The description can easily be extended to multistage amplifiers. Then the output matrix $\langle q_0 q_0^\dagger \rangle$ is the input matrix for the next stage.

4) The diagonal elements of the matrices $\langle q_0 q_0^\dagger \rangle$ and $\langle q_i q_i^\dagger \rangle$ contain information about the AM, FM, and bias current noise, while the off-diagonal elements contain information about the mutual correlation between these quantities. For example, the correlation between the AM and FM output noise is given by

$$C_{\mathrm{AM,FM}}^2 = \left| \frac{\langle q_{0-1}^* q_{00}^* \rangle \langle q_{00} q_{0-1} \rangle}{\langle q_{0-1} q_{0-1}^* \rangle \langle q_{00} q_{00}^* \rangle} \right| = \left| \frac{\langle i_C \delta\omega^* \rangle \langle i_C^* \delta\omega \rangle}{\langle i_C i_C^* \rangle \langle \delta\omega \delta\omega^* \rangle} \right|. \tag{22}$$

5) The theory presented here can also be used for studying the transfer of modulated signals, double sideband as well as single sideband, through the amplifier (see Section V).

IV. Comparison with Experiments on Locked Oscillators

AM and FM noise measurements were performed on single-stage circulator-coupled locked oscillators equipped with single-drift Si p^+-n diodes. In these oscillators branch II in the circuit of Fig. 2 consisted of a low-Q slug-tuned coaxial circuit. The noise measurements were carried out as described in [4]. The results presented here refer to double-sideband noise in a band of 100 Hz at a distance of f_m Hz from the carrier, as indicated.

All parameter values needed in the calculations were determined *a priori* from independent measurements as described in [15] and [19] to characterize the diode and its mount, and from calculations based on the experimental settings of the tuning slugs and the slug dimensions to characterize the circuit. The AM and FM noise of the input signal was taken as uncorrelated. The circulator was assumed to be ideal. As pointed out in Section II [see (12a)], the amount of noise calculated is rather sensitive to the value of det $\{S\}$. Hence in the calculations a self-consistent set of parameters has to be used. This can be achieved, for example, by requiring a calculation of the correct experimental oscillation frequency f_f and correct bias current I_{st} at the start of the oscillations of the *free-running* oscillator on the basis of the mentioned parameters, but allowing for a small adjustment of the circuit loss resistance and a small adjustment of a reactance in the embedding network. In the subsequent calculations of the locked oscillator noise no adjustable parameters are left and the only variables left are the locking frequency, the locking power, and the bias current. The values of the latter three quantities were taken as in the experiments. It should be noted that since all parameters are known now, no curve fitting is possible when comparing experimental and theoretical results of the locked oscillator noise. Results are presented for two locked oscillators, denoted by A[1] and B, respectively. Data of the diodes used are summarized in Table I, which also gives the starting conditions of the free-running oscillators ($P_i = 0$).

The measured and calculated effective noise figure F_{eff}[2] as a function of the output power of locked oscillator A is

[1] The authors are indebted to H. Tjassens for permission to use his experimental results for locked oscillator A.

[2] $F_{\mathrm{eff}} = (\Delta f_{\mathrm{rms}}^2 P_i)/(f_m^2 kTB)$, where Δf_{rms} is the rms frequency deviation of the output signal, k is Boltzmann's constant, and $T = 300$ K is taken.

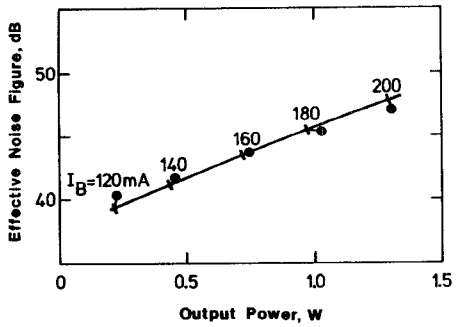

Fig. 4. Measured (dots) and calculated effective noise-figure F_{eff} as a function of the output power of locked oscillator A (Table I), with I_B as parameter ($f_L = f_f = 6.4$ GHz, $P_i = 5$ dBm, $f_m = 4$ MHz).

TABLE I
DIODE CHARACTERISTIC QUANTITIES AND FREE-RUNNING OSCILLATOR STARTING CONDITIONS

Locked Oscillator	A	B
Breakdown voltage (V)	103	66
l_a (μm)	2.0	1.2
l_d (μm)	4.5	1.9
C_o (pF)	1.1	0.44
$\bar{\alpha}'/\tau_i C_a$ ($A^{-1}sec^{-1}$)	$4.2\ 10^{21}$	$3.1\ 10^{22}$
τ_i (ps)	5.6	3.6
f_f (GHz)	6.4	9.5
I_{st} (mA)	110	22

given in Fig. 4. In this case $f_L = f_f = 6.4$ GHz, $P_i = 5$ dBm, and $f_m = 4$ MHz. The output power was varied by varying I_B as indicated in the figure. It is concluded that even at relatively high output levels the amplifier noise is well described by our theory. The remaining results to be presented concern the locked oscillator B. In the free-running state the diode in this oscillator operated at a modulation level $m = 0.12$, where m is the ratio of the total ac voltage across the diode to the breakdown voltage. The measured and calculated AM and FM noise, in terms of the double-sideband noise power-to-carrier power ratio, of the free-running oscillator is given in Fig. 5, as is the AM and FM noise of the locked oscillator as a function of $\Delta f_L = f_L - f_f$. In this case the locking gain $G = P_{out}/P_i = 30$ dB. The value of G was chosen as high as this in order to have a marked difference between the FM noise of the X-13 klystron used as input source and the output FM noise of the locked oscillator; see also Fig. 6. Except for a small difference in locking range, this experiment is also well described by our theory. The difference in locking range found might be attributed to the relatively simple diode model used [13]. It should be noted that the noise of the free-running and that of the locked oscillator was calculated using the same set of diode and circuit parameters.

The results for the AM and FM noise-to-carrier ratio as a function of the locking gain, with $f_L = f_f$, are given in Fig. 6. The locking gain was varied by varying the locking power only. The FM noise-to-carrier ratio of the input signal

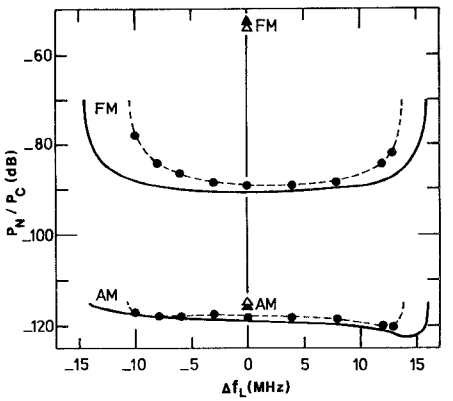

Fig. 5. Theoretical and experimental (dots) double-sideband noise power-to-carrier power ration of the AM and FM noise of locked oscillator B (Table I) as a function of the locking frequency, $\Delta f_L = f_L - f_f$, and that of the free-running oscillator at f_f (closed triangles experiment, open triangles theory). $G = 30$ dB, $f_L = 9.5$ GHz, $f_m = 200$ kHz.

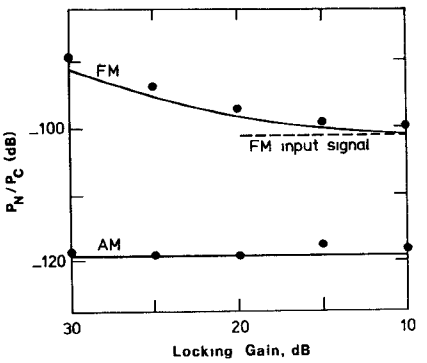

Fig. 6. AM and FM noise of locked oscillator A as a function of the locking gain, by variation of the input signal level. ($f_L = f_f = 9.5$ GHz, $f_m = 200$ kHz.) The FM noise level of the input signal is indicated by the broken line.

is indicated. The agreement between theory and experiment is good, also at higher input levels, i.e., lower values of G.

Though not measured for the present locked oscillator, it is well known [20, fig. 2] that near the carrier the FM noise of a locked oscillator follows that of the locking signal, while far away from the carrier the FM noise is determined by the free-running oscillator. This behavior is also predicted by our theory [21, fig. 5], including the flat intermediate part when expressing the FM noise in a noise-power to carrier-power ratio.

V. MODULATION AND CONVERSION

For the application of negative resistance amplifiers it is of importance to know to what extent AM noise or modulation of the input signal manifests itself as AM and FM noise or modulation in the output signal. Similarly, there is the question as to what extent the input FM is converted into output AM and FM. In this last section examples will be given to demonstrate that these phenomena can easily be studied with the present theory. The examples will be given for locked oscillator B.

In the first example it is assumed that in (21) only the 1-1 element of the $\langle q_i q_i^\dagger \rangle$ matrix is nonzero, i.e., it is

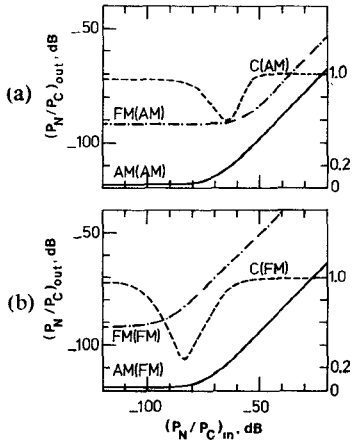

Fig. 7. Calculated output AM noise (fully drawn line) and FM noise (dash-dotted line), and their mutual correlation (broken line) as a function of the input noise of one type. Locked oscillator B, $G = 30$ dB, $f_m = 4$ MHz, double sideband, $B = 100$ Hz. (a) Input noise AM noise only. (b) Input noise FM noise only.

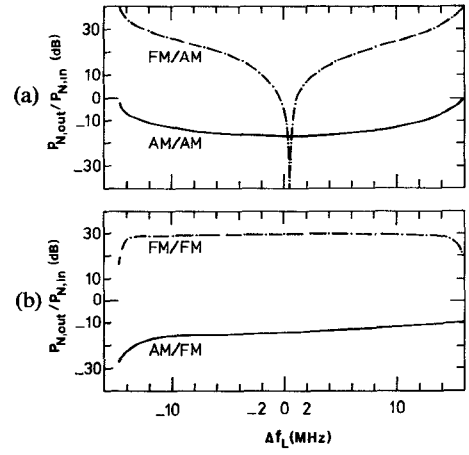

Fig. 8. Calculated output AM noise (fully drawn line) and FM noise (dash-dotted line) as a function of $\Delta f_L = f_L - f_f$. Input noise level so high that output AM and FM noise are fully correlated. Locked oscillator B as in Fig. 7. (a) Input noise AM noise only. (b) Input noise FM noise only.

assumed that the input signal has no FM noise or modulation, that it is purely AM modulated, and that there is no external bias current noise or modulation. Then in Fig. 7(a) the calculated AM and FM noise-power to carrier-power ratio of the output signal and the correlation coefficient between the output AM and FM noise are given as a function of the AM input noise-power to carrier-power ratio. Similarly, Fig. 7(b) shows these output quantities in the case where the input signal is purely FM modulated, i.e., only the 2-2 element of $\langle q_i q_i^\dagger \rangle$ is nonzero. For the results in Fig. 7, the values $f_L = f_f$, $G = 30$ dB, and $f_m = 4$ MHz apply. From Fig. 7 it is concluded that the output noise at low values of the input noise is fully determined by the noise generation inside the diode, while the correlation between output AM and FM is near unity [3]. Consequently, these results indicate the minimum noise obtainable with this oscillator in its present adjustment and, moreover, the maximum noise allowed on the input signal such that the output noise is not influenced by the noise on the input signal. For high values of the input noise, the output noise is fully determined by that input noise, while output AM and FM noise are fully correlated. Hence in these regions of high input noise the results for the output noise are fully determined by the transfer properties of the locked amplifier. In the example given, the changeover from noise to modulation takes place at an AM input level of about -60 dB and an FM input level of about -80 dB. At these levels a loss of correlation of the output AM and FM noise is observed, as is to be expected because then the input noise and the IMPATT diode noise are equally important.

Under the additional condition, with respect to the conditions leading to the results of Fig. 7, that the input noise of one type is at such a high level that the output AM and FM are fully correlated, the output noise has been calculated over the locking band. The results, as shown in Fig. 8, are presented in terms of

$$\frac{P_{N,\text{out}}}{P_{N,\text{in}}} = \frac{(P_N/P_C)_{\text{out}}}{(P_N/P_C)_{\text{in}}} \cdot G \tag{23}$$

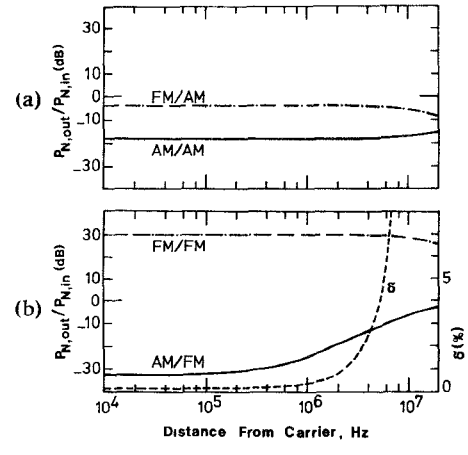

Fig. 9. As in Fig. 8 but as a function of the distance f_m from carrier, with $f_L = f_f$. The broken line in (b) represents the relative variation of the rms frequency deviation of the input signal to that of the output signal. (a) Input noise AM noise only. (b) Input noise FM noise only.

where the index N stands for AM or FM noise. In Fig. 8(a) the input signal is purely AM modulated, and in Fig. 8(b) it is purely FM modulated. In addition, Fig. 9 gives these modulation quantities as a function of f_m, when $f_L = f_f$. The results for $P_{\text{FM,out}}/P_{\text{AM,in}}$ [Figs. 8(a) and 9(a)], are a direct measure of the AM-to-PM conversion factor of the amplifier [21], where the sign of this factor can be found from a consideration of the angle between V_{i0} and I_{00} (Fig. 3) as a function of G. In the present example, this sign changes at $\Delta f_L \approx 0.5$ MHz, thus explaining the strong variation of $P_{\text{FM,out}}/P_{\text{AM,in}}$ at that frequency in Fig. 8(a). The ratio $P_{\text{FM,out}}/P_{\text{FM,in}}$ in Figs. 8(b) and 9(b) is a measure of the phase distortion of the amplifier. It can be concluded that this ratio does not vary much over the locking band or as a function of f_m when $f_L = f_f$. The value of this ratio is close to 30 dB, thus equal to the locking gain, indicating that the input and output signal have nearly the same rms frequency deviation. In our calculations we never met a situation in which $\Delta f_{\text{rms,out}}$ was exactly equal to $\Delta f_{\text{rms,in}}$,

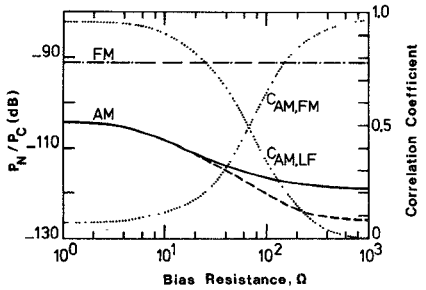

Fig. 10. Calculated output AM noise (fully drawn line) and FM noise (dash-dotted line) and AM noise on the current through the diode itself (broken line) as a function of the bias circuit resistance. The curve labeled $C_{AM,FM}$ represents the correlation between output AM and FM noise, that labeled $C_{AM,LF}$ the correlation between output AM noise and bias current noise. Locked oscillator B, $G = 30$ dB, $f_m = 4$ MHz, double sideband, $B = 100$ Hz. Input signal noise free.

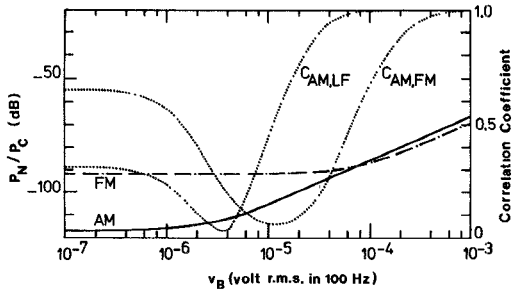

Fig. 11. As in Fig. 10 but as a function of the rms voltage v_B of an external noise source in series with $R_B = 100\ \Omega$.

indicating that some distortion of the FM modulation is always to be expected. As an example, the broken line in Fig. 9(b) represents $\delta(f_m)$, defined by

$$\delta(f_m) = \frac{\Delta f_{\text{rms,in}}(f_m) - \Delta f_{\text{rms,out}}(f_m)}{\Delta f_{\text{rms,in}}(f_m)} \cdot 100.$$

Near the carrier $\delta \approx 0.1$ percent, while δ increases rapidly for $f_m > 1$ MHz. Further conclusions of Figs. 7–9 are left to the reader.

In the preceding examples, the conditions were taken such that the influence of the noise or modulation present in the bias circuit was negligible. In the final two examples, the bias circuit will be drawn into the discussion. As shown in Fig. 10, a reduction of the bias resistance R_B brings on an increase of the output AM noise as a result of upconversion of the low-frequency noise generated in the avalanche process. The output FM noise showed hardly any increase when R_B was decreased. The noise description presented in this paper easily allows the consideration of the noise in various parts of the circuit. As an example, the broken line in Fig. 10 presents the AM noise on the current I_{t0} through the diode. It is concluded that at high values of R_B, where the influence of the bias current noise is negligible, the transformations involved when going from $I_{t0} \rightarrow I_{00}$ bring on a difference in the AM noise on these currents. Also given in Fig. 10 are the correlation coefficients $C_{AM,LF}$ and $C_{FM,AM}$, where the indices AM and FM are related to these types of noise on I_{00}.

Finally, Fig. 11 presents the results for the output AM and FM noise, their mutual correlation, and the correlation between AM noise and bias current noise, in the presence of an external noise source with rms voltage v_B, and frequency 4 MHz. In this example, $R_B = 100\ \Omega$ and the input signal is taken free of FM and AM noise, so only the 3-3 element of the matrix $\langle q_i q_i^\dagger \rangle$ is nonzero. It is found that high values of v_B influence not only the AM noise but also the FM noise. The correlation coefficients show the familiar behavior.

VI. Summary

The theory of noise in IMPATT diode oscillators at large-signal levels by Goedbloed and Vlaardingerbroek has been extended to allow a direct comparison with experiments concerning AM, FM, and bias current noise and/or modulation measurements on reflection-type IMPATT diode amplifiers. The theory allows for the study of conversion properties such as AM into AM and FM, etc., including the correlation coefficient between these quantities. Furthermore, the theory makes it possible to give values of the minimum output noise of a given amplifier configuration and, in addition, values of the maximum noise on the input signal without influencing the noise on the output signal. AM and FM noise measurements on injection-locked oscillators equipped with single-drift Si p^+-n diodes have been shown to be in good agreement with the theory.

The success of the present theoretical methods in connection with IMPATT diode studies on oscillator noise [3], amplifier properties, and spurious parametric signals [10], [11] suggests that application can be fruitful in the study of circuits equipped with other nonlinear devices as well, if only a practical large-signal theory is available along with a knowledge of the noise sources and their signal dependence.

Acknowledgment

The authors wish to thank H. Tjassens and H. F. Tack for valuable discussions, and H. G. Kock and J. G. A. den Biggelaar for fabricating the diodes.

References

[1] G. Convert, "Sur la theorie du bruit des diodes à avalanche," *Rev. Tech. Thomson-CSF*, vol. 3, pp. 419–471, 1971.
[2] M. E. Hines, "Large-signal noise, frequency conversion, and parametric instabilities in IMPATT-diode networks," *Proc. IEEE*, vol. 60, pp. 1534–1548, Dec. 1972.
[3] J. J. Goedbloed and M. T. Vlaardingerbroek, "Noise in IMPATT-diode oscillators at large signal levels," *IEEE Trans. Electron Devices*, vol. ED-21, pp. 342–351, June 1974.
[4] J. J. Goedbloed, "Noise in IMPATT-diode oscillators," *Philips Res. Rep. Supplements*, no. 7, 1973.
[5] A. Mircea, E. Constant, and R. Perichon, "FM noise of high-efficiency GaAs IMPATT oscillators and amplifiers," *Appl. Phys. Lett.*, vol. 26, pp. 245–247, 1975.
[6] M. T. Vlaardingerbroek, "On the signal dependence of avalanche noise generation," *IEEE Trans. Electron Devices*, vol. ED-22, pp. 309–313, June 1975.
[7] H. A. Haus, R. A. Pucel, and H. Statz, "Noise in IMPATT diodes under large signal conditions," *Proc. 4th Int. Conf. on Physical Aspects of Noise in Solid-State Devices*, pp. 104–107, Noordwijkerhout, Sept. 1975.
[8] R. Adler, "A study of locking phenomena in oscillators," *Proc. IRE*, vol. 34, pp. 351–357, June 1946.
[9] K. Kurokawa, "Injection locking of microwave solid-state oscillators," *Proc. IEEE*, vol. 61, pp. 1386–1410, Oct. 1973.
[10] J. J. Goedbloed and H. Tjassens, "Parasitic oscillations in IMPATT diode oscillators," *Proc. 4th European Microwave Conf.*, pp. 328–332, Montreux, Sept. 1974.

[11] W. E. Schroeder, "Spurious parametric oscillations in IMPATT-diode circuits," *Bell Syst. Tech. J.*, vol. 53, pp. 1187–1210, Sept. 1974.
[12] J. J. Goedbloed, "Investigation of parasitic oscillations in IMPATT-diode oscillators by a simple locus chart," *Electron. Lett.*, vol. 11, pp. 54–56, Feb. 1975.
[13] L. J. Meuleman, "Injection frequency locking of the avalanche transit-time oscillator," *Philips Res. Rep.*, vol. 27, pp. 201–222, 1972.
[14] T. Berceli, "Nonlinear effects in IMPATT diode amplifiers," *Proc. 5th European Microwave Conf.*, pp. 705–709, Hamburg, Sept. 1975.
[15] J. J. Goedbloed, "Determination of the intrinsic response time of semiconductor avalanches from microwave measurements," *Solid-State Electron.*, vol. 15, pp. 635–647, 1972.
[16] K. M. Brown, "Solution of simultaneous non-linear equations," *Comm. ACM*, vol. 10, pp. 728–729, Nov. 1967.
[17] E. S. Kuh and R. A. Rohrer, *Theory of Linear Active Networks.* San Francisco: Holden-Day Inc., ch. 6, 1967.
[18] J. L. Fikart and P. A. Goud, "A theory of oscillator noise and its application to IMPATT diodes," *J. Appl. Phys.*, vol. 44, pp. 2284–2296, 1973.
[19] B. B. van Iperen and H. Tjassens, "Novel and accurate methods for measuring small-signal and large-signal impedances of IMPATT diodes," *Philips Res. Rep.*, vol. 27, pp. 38–75, 1972.
[20] I. Tatsuguchi, N. R. Dietrich, and C. B. Swan, "Power-noise characterization of phase-locked IMPATT oscillators," *IEEE J. Solid-State Circ.*, vol. SC-7, pp. 2–10, Feb. 1972.
[21] J. J. Goedbloed and M. T. Vlaardingerbroek, "Noise and modulation properties of IMPATT diode amplifiers," *Proc. 5th European Microwave Conf.*, pp. 685–689, Hamburg, Sept. 1975.
[22] R. D. Kuvås, "Nonlinear noise theory for IMPATT diodes," *IEEE Trans. Electron Devices*, vol. ED-23, pp. 395–411, Apr. 1976.

Short Papers

The Aerospace Low-Noise Millimeter-Wave Spectral Line Receiver

WILLIAM J. WILSON

Abstract—**A multichannel millimeter-wave receiver has been designed and built to study narrow-band signals from the natural background. This receiver is used with the Aerospace 4.6-m millimeter-wave antenna at El Segundo, CA. It is a superheterodyne mixer receiver which will tune over the 70–120-GHz frequency range with a system noise temperature of ~500 K (DSB).**

The spectral line receiver includes the RF system, the IF system, the local oscillator (LO) phase-locking system, the multichannel filter receivers, and the data processing system. This short paper describes the design and operation of the spectral line receiver and provides a sample of the results obtained.

I. Introduction

A multichannel millimeter-wave receiver has been designed and built to study narrow-band signals from molecules in the interstellar medium and in planetary (including the earth's) atmospheres. These weak noise signals are concentrated in bandwidths of 100 kHz–10 MHz with received antenna temperatures ranging from 10^{-3} to 10^{2} K. This receiver is used with the Aerospace 4.6-m millimeter-wave radio telescope located in El Segundo, CA [1]. The receiver is a superheterodyne type which will tune over the 70–120-GHz frequency range with a system noise temperature of ~500 K (DSB), making it one of the world's lowest noise room-temperature receivers at millimeter wavelengths.

The spectral line receiver includes the RF system, the IF system, the local oscillator (LO) phase-locking system, the multichannel filter receivers, and a computer-controlled data processing system. A block diagram of the receiver is shown in Fig. 1 and a picture of the control room in Fig. 2.

The ~100-GHz signal is received by a feed horn located at the antenna's Cassegrain focus, where it passes through the LO injection filter to the room-temperature single-ended mixer. The mixer downconverts the signal to 1.38 GHz, where it is amplified by an uncooled parametric amplifier which has a noise temperature of ~45 K and a bandwidth of 100 MHz. The signal is further amplified by transistor amplifiers and then sent to the receiver control room. In the control room, the signal is filtered, amplified, and converted to 150 MHz, and distributed to the filter receivers and a total power/synchronous detector receiver. All receiver tuning adjustments are servo controlled at the radiometer control panel. The millimeter-wave local oscillator klystron (located in the antenna equipment box) is phase locked to a ~100-MHz frequency synthesizer (in the control room), which sets the precise operating frequency. Using this phase-locking system, the klystron can be switched over a 100-MHz frequency range at a 10-Hz rate. The LO signal is sent to the mixer through a LO injection filter, which serves to minimize signal and LO losses and also to filter the LO signal.

Two multichannel filter receivers are used to analyze the received signal. A 64-channel 1-MHz bandwidth-per-channel filter receiver is used to analyze wide bandwidth signals, and a 128-channel 250-kHz bandwidth-per-channel receiver is used to obtain narrow frequency resolution of the incoming signals. The outputs of the filter banks are sent to a 192-channel multiplexer

Manuscript received June 1, 1976; revised September 28, 1976. This work was performed under a company-sponsored research program of millimeter-wave measurements.
The author was with the Electronics Research Laboratory, The Aerospace Corporation, El Segundo, CA 90250. He is now with the Department of Electrical Engineering, University of Texas, Austin, TX 78712.